Microscopic composition of ion-ion interaction potentials

A. S. Umar,[1] V. E. Oberacker,[1] J. A. Maruhn,[2] and P.-G. Reinhard[3]
[1]*Department of Physics and Astronomy, Vanderbilt University, Nashville, Tennessee 37235, USA*
[2]*Institut für Theoretische Physik, Goethe-Universität, D-60438 Frankfurt am Main, Germany*
[3]*Institut für Theoretische Physik, Universität Erlangen, D-91054 Erlangen, Germany*
(Received 8 October 2011; published 4 January 2012)

We present a new method to calculate the total ion-ion interaction potential in terms of building blocks, which we refer to as "single-particle interaction potentials." This allows also the composition of the separate contributions of neutrons and protons to the interaction potentials. The method is applied to nuclear collisions via the use of time-dependent Hartree-Fock theory.

DOI: 10.1103/PhysRevC.85.017602 PACS number(s): 21.60.Jz, 25.60.Pj, 25.70.−z

Introduction. The knowledge of interaction potentials between composite many-body systems is of fundamental importance for predicting the outcome of reactions involving such entities. These are often modeled using empirical functions that depend on macroscopic variables, such as the distance between the two centers, treating the composite objects as structureless particles and ignoring the microscopic origins of these potentials (e.g., Lennard-Jones potential for rare-gas atoms [1] and nucleon-nucleon potentials [2]). On the other hand, microscopic approaches try to obtain such potentials by including the interactions of the constituents, such as the building blocks, and calculating the whole potential as a function of some set of macroscopic variables (e.g., Born-Oppenheimer approximation for molecules [3] and deformed shell models for nuclei [4]). However, the total potential obtained this way does not reveal the contribution coming from individual single-particle states. Quoting Schrödinger, the "best knowledge of a whole does not necessarily include [the] best possible knowledge of the parts." The entanglement of these contributions may yield further insight as to the interaction of many-body systems via a representative potential.

Most common microscopic approaches for calculating interaction potentials usually employ the adiabatic or sudden approximations for the relative motion of the interacting systems [5]. Recently, we have introduced a new microscopic approach for the calculation of ion-ion potentials for nuclear collisions. This method is based on the time-dependent Hartree-Fock (TDHF) description of nuclear collisions coupled [6] with a constraint on the local density at the given instant of time. Interaction potentials obtained using the so-called density-constrained-TDHF (DC-TDHF) method [7] have been successful in describing fusion cross sections for a number of systems [8]. The new approach we will describe below is generally suitable for microscopic calculations provided Koopmans' theorem [9] is applicable.

Formalism. The microscopic approaches based on the mean-field approximation often use the energy difference between the combined system and the asymptotic energies of the individual systems to calculate the ion-ion interaction potential as

$$V(R) = E_{A_1+A_2}(R) - E^{(0)}_{A_1} - E^{(0)}_{A_1}, \tag{1}$$

where $E_{A_1+A_2}(R)$ is the total energy obtained for the combined system as a function of the distance R between the two ions and $E^{(0)}_{A_i}$ are the individual binding energies of the two systems calculated using the same interaction. The binding energies are often calculated either by integrating the energy density over all space $E = \int d^3r\mathcal{H}(\boldsymbol{r})$ or via Koopmans' expression $E = \frac{1}{2}\sum_\alpha w_\alpha(t_\alpha + \epsilon_\alpha)$, where w_α denotes the occupation probability of the single-particle state α. This mixture of half kinetic energies t_α and half single-particle energies ϵ_α applies to Hartree-Fock calculations employing purely two-body forces. For mean-field calculations based on density-dependent effective forces [10] or energy-density functionals [11], a rearrangement term needs to be added to the above expression [12]. This can be disentangled to single-particle energies and a rearrangement term as

$$E = \frac{1}{2}\sum_\alpha w_\alpha(t_\alpha + \epsilon_\alpha) - \frac{1}{2}\mathrm{Tr}\left(\langle \mathrm{HF}|\frac{\delta v}{\delta\rho}|\mathrm{HF}\rangle\rho\right), \tag{2}$$

where v is the density-dependent part of the interaction. We can deduce a generalized single-particle sum from this by decomposing the second ρ in the rearrangement term into single-particle densities as $\rho = \sum_\alpha \rho_\alpha$, yielding

$$E = \frac{1}{2}\sum_\alpha w_\alpha(t_\alpha + \epsilon_\alpha + \tilde{\epsilon}_\alpha), \tag{3}$$

where $\tilde{\epsilon}_\alpha$ is the single-particle rearrangement energy arising from the above modification. All of the binding energies comprising the ion-ion interaction potential via Eq. (1) can be expressed using the above form. In terms of these expressions the ion-ion interaction potential can be represented as a sum over single-particle interaction potentials as

$$V(R) = \sum_\alpha w_\alpha v_\alpha(R) \tag{4}$$

with

$$v_\alpha(R) = \tfrac{1}{2}\left[(t_\alpha + \epsilon_\alpha + \tilde{\epsilon}_\alpha)(R) - \left(t^0_\alpha + \epsilon^0_\alpha + \tilde{\epsilon}^0_\alpha\right)\right], \tag{5}$$

where the quantities with the superscript 0 denote the asymptotic values. This decomposition is sensible if the single-particle energies are good representatives of the corresponding

separation energies according to Koopmans' theorem [9] and if the rearrangement corrections remain small. Such a situation is given in the application example discussed below, namely, nuclear mean-field calculations using Skyrme forces. In this case, the proton and neutron interaction potentials are obtained simply by summing the single-particle potentials $v_\alpha(R)$ over all protons or neutrons, respectively. Strictly speaking, Koopmans' theorem applies only to closed-shell nuclei, and it remains valid only if there are no dramatic changes in deformation when removing one particle. However, it is generally found to be a good approximation for light nuclei where pairing forces are negligible. For heavier systems where pairing interactions become sizable, the formalism can only be used for systems near closed shells where the pairing gap vanishes. For electronic energy-density functionals, one has to employ a self-interaction correction to restore Koopmans' theorem approximately [13,14].

Results. For the application of the above concepts we have used the DC-TDHF approach [7]. In this approach TDHF time evolution takes place with no restrictions. At certain times during the evolution, the instantaneous densities $\rho_{p/n}(\boldsymbol{r}, t)$ are used to perform a static Hartree-Fock minimization while holding the neutron and proton densities constrained to be the instantaneous TDHF densities [15]. In essence, this introduces the concept of an adiabatic reference state for a given TDHF state. The difference between these two energies represents the internal energy. The adiabatic reference state is the one obtained via the density-constraint calculation, which is the Slater determinant with lowest energy for the given density with vanishing current and approximates the collective potential energy after the subtraction of the static binding energies as shown in Eq. (1). All of the dynamical features included in TDHF are naturally included in the DC-TDHF calculations.

In practice, we have used the Skyrme SLy4 effective nuclear interaction [16] for our calculations. The rearrangement terms described above can be written as

$$\tilde{\epsilon}_\alpha = \tilde{\epsilon}_\alpha^{(3)} + \tilde{\epsilon}_\alpha^{(C)} + \tilde{\epsilon}_\alpha^{(\mathrm{DC})} \tag{6}$$

with

$$\tilde{\epsilon}_\alpha^{(3)} = -\frac{\gamma}{12} t_3 \int d^3r \rho_\alpha \rho^{\gamma-1} \left[\left(1 + \frac{x_3}{2}\right) \rho^2 - \left(\frac{1}{2} + x_3\right) \left(\rho_n^2 + \rho_p^2\right) \right],$$

$$\tilde{\epsilon}_\alpha^{(C)} = -\frac{1}{2} \left(\frac{3}{\pi}\right)^{\frac{1}{3}} e^2 \int d^3r \rho_\alpha \rho_p^{\frac{1}{3}}, \quad \alpha \in \{\text{protons}\},$$

$$\tilde{\epsilon}_\alpha^{(\mathrm{DC})} = -\frac{1}{2} \int d^3r \rho_\alpha \lambda_{n,p}(\boldsymbol{r}),$$

where we have defined $\rho_\alpha = \psi_\alpha^*(\boldsymbol{r})\psi_\alpha(\boldsymbol{r})$ and $\lambda(\boldsymbol{r})$ is the coordinate-dependent Lagrange multiplier for the density constraint [15]. The subscripts n and p in the rearrangement term for the density constraint indicate a choice corresponding to the isospin content of the index α. The summation over α

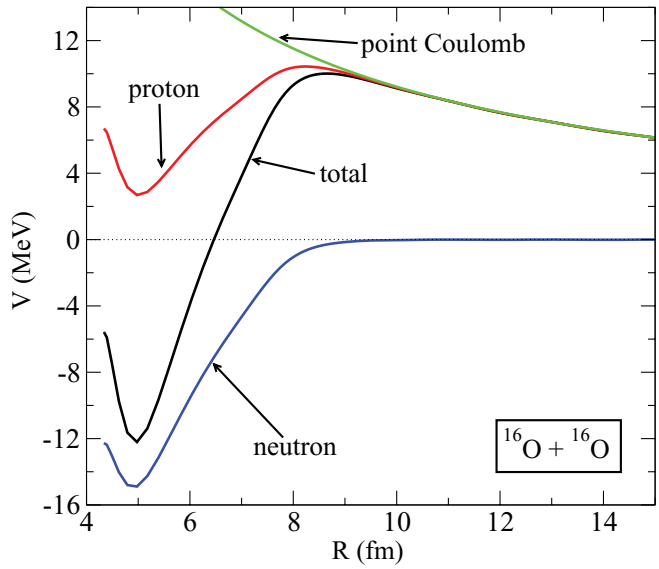

FIG. 1. (Color online) Interaction potential for a head-on collision of ^{16}O+^{16}O at $E_{\mathrm{cm}} = 12$ MeV. The black curve is the total ion-ion interaction potential. The red and blue curves show the contribution to the total potential coming from protons and neutrons, respectively. Also shown is the point Coulomb potential.

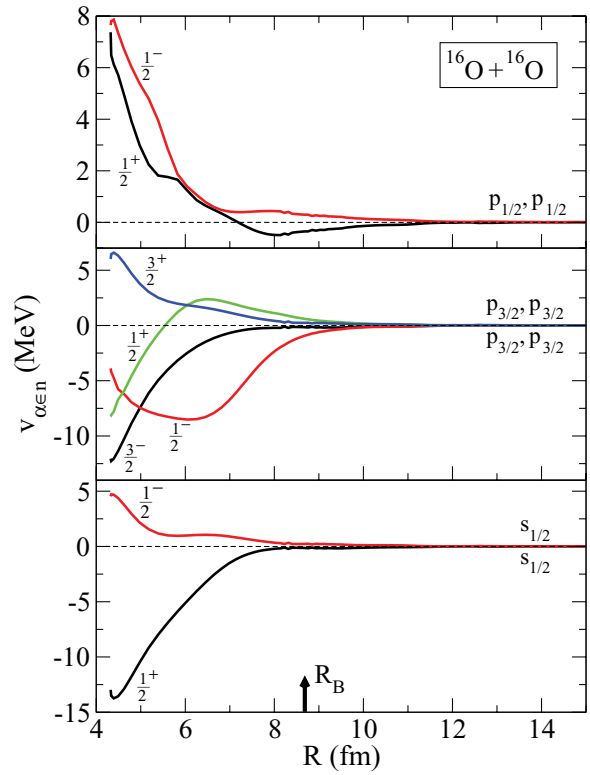

FIG. 2. (Color online) Contribution of neutron single particles to the interaction potential for a head-on collision of ^{16}O+^{16}O at $E_{\mathrm{cm}} = 12$ MeV. The sum of all these potentials gives the neutron curve in Fig. 1. The arrow marked R_B indicates the barrier top of the total potential shown in Fig. 1.

exactly reproduces the total rearrangement energies obtained by direct integration.

The first collision studied is ^{16}O+^{16}O at $E_{cm} = 12$ MeV. In Fig. 1 we show the total interaction potential (black curve) as well as the contributions coming from neutrons and protons to this total potential. The total interaction potential is numerically identical to the one obtained in standard DC-TDHF calculations using the integral of the energy density to obtain the terms in Eq. (1). In general, DC-TDHF calculations show that the ion-ion potential depends on the energy E_{cm}. For light systems like ^{16}O+^{16}O, the energy dependence is found to be negligible (see Ref. [17], Fig. 1), but for heavier systems such as ^{16}O+^{208}Pb [8] and ^{48}Ca+^{238}U [18], the energy dependence is appreciable. The individual neutron and proton contributions were obtained by doing the α summation over the neutron and proton single-particle orbitals, respectively. As a reference we also show the point Coulomb interaction. As can be seen from the figure, the outer part of the potential barrier is primarily determined by the interaction potential between the protons of the two nuclei while the neutron potential is essentially zero. In other words the neutron-proton interaction does not influence the outer-barrier region. While inside the barrier, neutrons provide all of the attraction, and the proton potential remains positive for all R values.

In Fig. 2 we show the individual neutron single-particle potentials for the ^{16}O+^{16}O system. In spite of using three-dimensional Cartesian coordinates, we are able to calculate some quantum numbers when the solution possesses good symmetry. In this case, spherical initial ^{16}O nuclei allow the use of spherical quantum labels at the asymptotic position of the two nuclei. On the other hand, when the nuclei overlap, the system becomes approximately axially symmetric, thus allowing the computation of parity and the z component of the total angular momentum. The reassignment of parities and the behavior of the states as they evolve toward smaller R values are noteworthy. For smallest R values the filling of the levels resembles that for a single-centered 32-particle system. The trend seen in the actual single-particle energies is relatively easy to understand; the two oxygen nuclei are initially far apart and are brought together. While they are far apart and isolated, the nuclei have identical energy levels. However, as the separation between the two nuclei becomes smaller, the single-particle states begin to overlap. The Pauli principle dictates that no two nucleons in an interacting system may have the same quantum state. Therefore, each (doubled) energy level of the isolated nuclei splits into two orbitals, one lower in energy than the original level and one higher. This can be most easily seen for the two initial $1s_{1/2}$ states. However, in addition to energy splitting, the parity of one of these states also changes from positive to negative since no more than two neutrons can be in the $1s_{1/2}$ state. (Each state is originally occupied by two neutrons, $w_\alpha = 2$.) In the language of molecular physics, the states that attain a lower energy than their asymptotic value are referred to as bonding states whereas the states that evolve to a higher energy are antibonding states [3].

In the case of nuclear reactions leading to fusion, bonding states are the states driving the system toward fusion whereas antibonding states resist the fusion process. We observe that not all neutron states are bonding states, but to the contrary about half are actually antibonding in character for small R values. One of the $p_{3/2}$ states [green (gray) curve] makes a transition from antibonding to bonding for smaller R values. Another manifestation of the bonding and antibonding states is their spatial localization. Bonding states are localized in the interior part of the combined system as opposed to antibonding states that are more spread out as can been seen from the single-particle moments. The time-dependent wave functions in TDHF are conceptually very different from the adiabatic

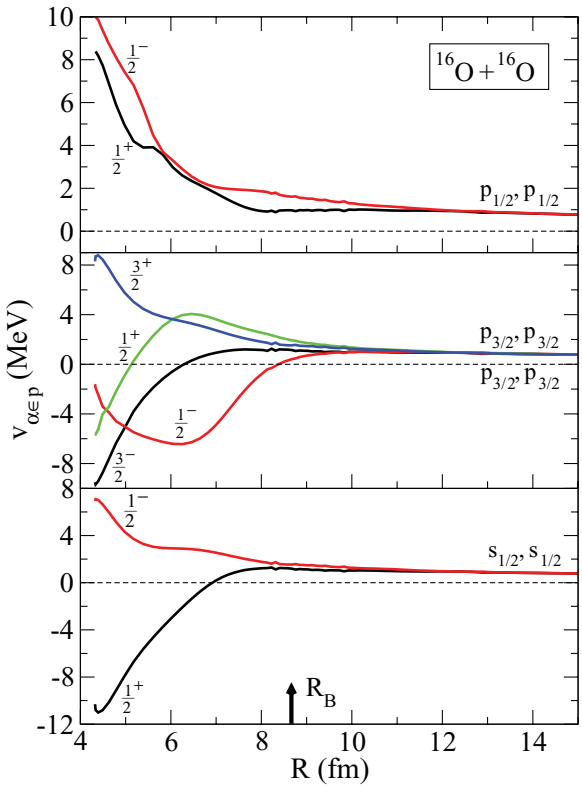

FIG. 3. (Color online) Same as Fig. 2 but for protons.

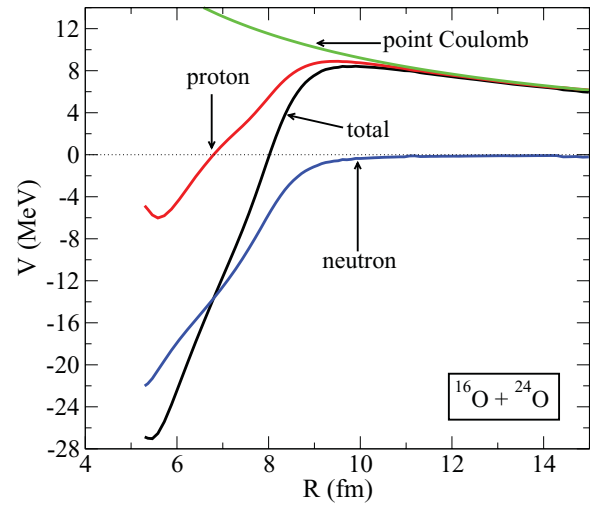

FIG. 4. (Color online) Interaction potential for a head-on collision of ^{16}O+^{24}O at $E_{cm} = 12$ MeV.

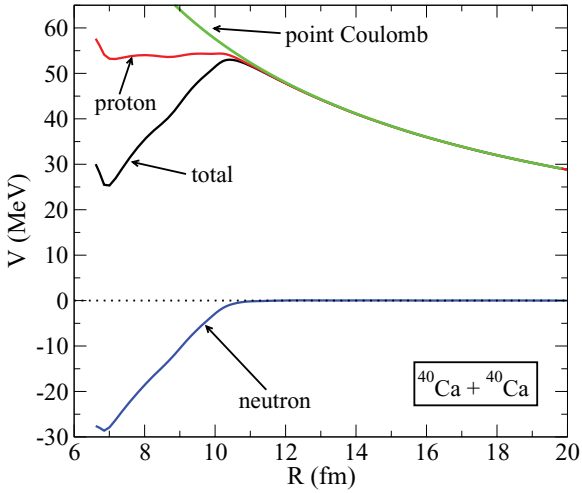

FIG. 5. (Color online) Same as Fig. 4 but for a head-on collision of ^{40}Ca+^{40}Ca at $E_{cm} = 55$ MeV.

basis states of the two-center shell model (TCSM), being very complicated superpositions of these, and a comparison is meaningful only in the initial phase of very low-energy reactions [19].

Figure 3 shows the contribution of proton single-particle states to the total ion-ion potential. The trend of the proton states is essentially the same as that of the neutron states with the exception of the rise from the zero-potential line (dotted lines) due to the presence of the Coulomb interaction. The sum of all these proton single-particle potentials reproduces the point Coulomb potential for the two incoming nuclei as can be observed in Fig. 1.

We have also performed calculations for head-on collisions of ^{16}O+^{24}O at $E_{cm} = 12$ MeV and for ^{40}Ca+^{40}Ca at $E_{cm} = 55$ MeV. In Fig. 4 we show the neutron and proton potentials for the ^{16}O+^{24}O system. We note that in comparison to the ^{16}O+^{16}O system, the potential minimum is considerably lower due to the presence of eight extra neutrons. The surplus bending from the extra neutrons also affects the proton potential, bringing it down to negative values for small R. We also note that the neutron potential starts its dip to negative values at larger R values than the ^{16}O+^{16}O case, thus bringing the total barrier maximum to a lower value. Figure 5 shows the same quantities for the ^{40}Ca+^{40}Ca system. The behavior of the proton potential is significantly different in this case. Inside the barrier the proton potential is essentially constant, and it only rises as the minimum value of R is reached. This is probably due to the stronger Coulomb potential which counterweights the nuclear binding. While the neutron and total potentials appear intuitively as expected, the proton potential behaves in an unexpected manner. This difference is due to the fact that here we are dealing with a finite-extent charge distribution at a microscopic level and not the point-charge Coulomb potential.

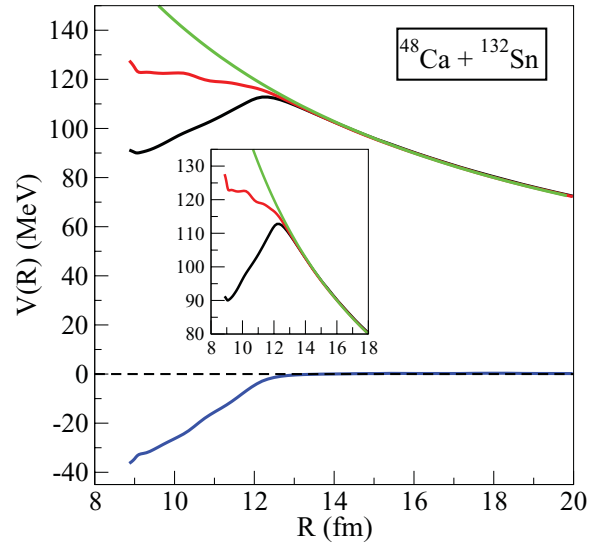

FIG. 6. (Color online) Same as Fig. 4 but for a head-on collision of ^{48}Ca+^{132}Sn at $E_{cm} = 120$ MeV. The insert magnifies the barrier-top region.

This is further evidence that the total potential may be masking some interesting features of its building blocks. In order to further explore the proton-potential behavior, we have repeated our calculations for a heavier system ^{48}Ca+^{132}Sn at $E_{cm} = 120$ MeV. In Fig. 6 we show the breakdown of the total ion-ion potential to neutron and proton parts for this collision. We observe that in this case the proton potential actually rises for smaller R values in comparison to the ^{40}Ca+^{40}Ca case, which can be more clearly seen in the insert of Fig. 6.

Conclusions. We have introduced a general approach for the calculation of single-particle interaction potentials as the building blocks of the total interaction potential for two fragments of finite fermion systems. The formulation is general provided Koopmans' theorem is applicable to the underlying energy functional used for the many-body calculations. The formalism is applied to calculate ion-ion potentials for nuclear reactions using TDHF for the time evolution of the nuclear collision together with the density-constraint formalism to find the corresponding adiabatic reference state. We show the contribution of single-particle potentials to the total potential for the ^{16}O+^{16}O case. We identify repulsive and attractive contributions as bonding and antibonding states, respectively. Perhaps the more obvious aspect is the identification of neutron and proton contributions to the total potential wherein we see clearly the subtle interplay between Coulomb repulsion and nuclear attraction for the protons while neutrons are always the dominant contributors to binding.

Acknowledgments. This work has been supported by the US Department of Energy under Grant No. DE-FG02-96ER40963 with Vanderbilt University and by the German BMBF under Contracts No. 06FY9086 and No. 06ER142D.

[1] N. W. Ashcroft and N. D. Mermin, *Solid State Physics* (Holt, Rinehart, and Winston, New York, 1976).

[2] R. Machleidt and I. Slaus, J. Phys. G: Nucl. Part. Phys. **27**, R69 (2001).

[3] M. Weissbluth, *Atoms and Molecules* (Academic, New York, 1978).
[4] M. Brack, J. Damgård, A. S. Jensen, H. C. Pauli, V. M. Strutinsky, and C. Y. Wong, Rev. Mod. Phys. **44**, 320 (1972).
[5] Amand Faessler, M. Ismail, N. Ohtsuka, M. Rashdan, and W. Wadia, Z. Phys. A **326**, 501 (1987).
[6] J. W. Negele, Rev. Mod. Phys. **54**, 913 (1982).
[7] A. S. Umar and V. E. Oberacker, Phys. Rev. C **74**, 021601(R) (2006).
[8] A. S. Umar and V. E. Oberacker, Eur. Phys. J. A **39**, 243 (2009).
[9] T. Koopmans, Physica (Amsterdam) **1**, 104 (1933).
[10] M. Bender, P.-H. Heenen, and P.-G. Reinhard, Rev. Mod. Phys. **75**, 121 (2003).
[11] R. M. Dreizler and E. K. U. Gross, *Density Functional Theory: An Approach to the Quantum Many-Body Problem* (Springer-Verlag, Berlin, 1990).
[12] P. Ring and P. Schuck, *The Nuclear Many-Body Problem* (Springer-Verlag, New York, 1980).
[13] J. P. Perdew and A. Zunger, Phys. Rev. B **23**, 5048 (1981).
[14] J. Messud, P. M. Dinh, P.-G. Reinhard, and E. Suraud, Phys. Rev. Lett. **101**, 096404 (2008).
[15] R. Y. Cusson, P.-G. Reinhard, M. R. Strayer, J. A. Maruhn, and W. Greiner, Z. Phys. A: At. Nucl. **320**, 475 (1985).
[16] E. Chabanat, P. Bonche, P. Haensel, J. Meyer, and R. Schaeffer, Nucl. Phys. A **635**, 231 (1998); **643**, 441(E) (1998).
[17] A. S. Umar, V. E. Oberacker, J. A. Maruhn, and P.-G. Reinhard, Phys. Rev. C **80**, 041601(R) (2009).
[18] A. S. Umar, V. E. Oberacker, J. A. Maruhn, and P.-G. Reinhard, Phys. Rev. C **81**, 064607 (2010).
[19] L. Guo, J. A. Maruhn, and P.-G. Reinhard, Phys. Rev. C **76**, 014601 (2007).